coatings

MDPI

Article

Preparation and Super-Hydrophobic Mechanism Analysis of FAS-17-Modified SiO_2/PDMS Coatings for High-Voltage Composite Insulators

Chengqian Li [1], Peng Dou [2], Ruyi Zhao [3], Yurou Shi [1], Gaojie Fu [1] and Bin Shen [1,*]

[1] School of Chemistry and Chemical Engineering, Southeast University, Nanjing 210096, China
[2] Jiangsu Frontier Electric Technology Co., Ltd., Nanjing 210000, China
[3] Shanghai Electro-Mechanical Engineering Institute, Shanghai 201109, China
* Correspondence: binshen@seu.edu.cn

Abstract: Pollution flashover on insulators is one of the greatest challenges affecting the smooth operation of high-voltage transmission lines. Demonstrating super-hydrophobic coatings on insulators' interfaces is an effective measure to prevent insulator flashovers. In the present investigation, a super-hydrophobic FAS-17-modified SiO_2/PDMS coating on a composite insulator was demonstrated by spraying. The coating had a contact angle of 159.2° and a sliding angle of 1.3° with better insulation properties. The prepared FAS-17-modified nano-SiO_2 nanoparticles were not easy to agglomerate; to illustrate this, the binding energy was calculated by the density functional theory. The super-hydrophobic mechanism of the coating was explained in terms of the adsorption energy between SiO_2 molecules and water before and after modification. This paper provides a new method to solve the pollution flashover problem of insulators and a new angle to explain the super-hydrophobic mechanism.

Keywords: super-hydrophobic; composite insulators; FAS-17-modified SiO_2 nanoparticles; de-agglomeration mechanism; super-hydrophobic mechanism; density functional theory

check for updates

Citation: Li, C.; Dou, P.; Zhao, R.; Shi, Y.; Fu, G.; Shen, B. Preparation and Super-Hydrophobic Mechanism Analysis of FAS-17-Modified SiO_2/PDMS Coatings for High-Voltage Composite Insulators. *Coatings* **2023**, *13*, 563. https://doi.org/10.3390/coatings13030563

Academic Editor: Fabio Palumbo

Received: 31 January 2023
Revised: 28 February 2023
Accepted: 1 March 2023
Published: 6 March 2023

Copyright: © 2023 by the authors. Licensee MDPI, Basel, Switzerland. This article is an open access article distributed under the terms and conditions of the Creative Commons Attribution (CC BY) license (https://creativecommons.org/licenses/by/4.0/).

1. Introduction

Electricity has become a necessity, and failing to keep the high-voltage transmission line running smoothly causes huge economic losses [1–3]. Previous reports have shown that the vast majority of electrical accidents were caused by insulator pollution flashovers [4–6]. Thus, finding ways to keep insulators clean is important to making high-voltage transmission lines run smoothly.

The main component of pollution on insulators is an inorganic salt (mainly NaCl and $CaSO_4$) [7–10], the accumulation of which increases the conductivity. Under the action of water and the electric field [11], the surface of insulators is discharged [1], and in serious cases, a large area of the power grid is cut off, bringing great economic losses to the power system. At present, the methods of cleaning insulators are as follows: laser cleaning [12], dry-ice cleaning [13], artificial spray cleaning [14], etc. The applications of laser cleaning and dry-ice cleaning are limited because the equipment is not suitable for the field environment. Currently, the main cleaning method is still for electric workers to flush the insulator with a high-pressure water gun [15], which has great potential for safety hazards. Therefore, it is better to build a protective coating on the surface of the insulator than to remove the pollution after it accumulates.

Super-hydrophobic coatings are often used as antifouling protective coatings because of their unique self-cleaning properties [16–18]. Coatings with contact angles greater than 150° and sliding angles less than 10° are called super-hydrophobic coatings [19,20]. Super-hydrophobic coatings consist of two parts. One is the low-surface-tension polymer substrate, and the other is the nanoparticles with higher roughness [21,22]. Polymer materials

used as low-surface-tension substrates can be classified as fluorinated long-chain hydrocarbons and fluorine-free long-chain hydrocarbons. Hydrocarbons with fluorinated long chains, such as polyvinylidene difluoride (PVDF), poly tetra fluoroethylene (PTFE), and poly(3-trifluoroethoxymethyl-3-ethyloxetane) (P3F), can greatly reduce the surface energy to meet the requirements of super-hydrophobic material substrate layer [23–26]. The prominent shortcomings of fluorine-rich coatings are their high prices and non-biodegradable nature [27]. Therefore, fluorinated long-chain hydrocarbons are not suitable for use as substrates on a large scale. Because of the significant shortcomings of fluorocarbons, fluorine-free polymers are more suitable as the base material for making super-hydrophobic coatings. In recent reports, polydimethylsiloxane (PDMS) elastomers have emerged as excellent representatives of fluorine-free polymers [28]. This kind of elastomer has a certain transparency, strong flexibility, good mechanical elasticity, lower cost than fluoro-containing polymers, and good adhesion on various substrate surfaces [29,30]. The surface tension (20 mN/m) of PDMS is relatively low [29], and the chemical properties of PDMS are stable [31]. Owing to these advantages, PDMS is suitable to be selected as the substrate. As for the choice of nanoparticle, nano-SiO_2 [32], nano-Fe_2O_3 [33], and nano-Al_2O_3 [34] are common choices. Considering the insulators are used in a high-voltage transmission line, the breakdown voltage is an important parameter to measure. According to a previous report, SiO_2 has a proper breakdown voltage [35]. However, small nano-SiO_2 particles tend to aggregate into larger particles, which affects the stability and flatness of the coating surface [36]. In order to ease the agglomeration of nanoparticles (NPs), the introduction of long-chain molecules on the surface of SiO_2 is a common method [37,38]. Xue Dai et al. constructed a super-hydrophobic porous SiO_2@PDMS protective layer using the spraying method with a contact angle of 155° [39], indicating that the contact angle can increase to reach better self-cleaning performance. O. Rius-Ayra et al. fabricated a super-hydrophobic PDMS@304 stainless-steel mesh using a chemical etching method [40]. The contact angle of the PDMS@304 stainless-steel mesh reached 159°, but the method used a large number of toxic and harmful chemicals, which is not environmentally friendly.

Therefore, based on the previous research, we designed a super-hydrophobic coating that is environmentally friendly and has a larger contact angle. In our work, 1H, 1H, 2H, 2H-perfluorodecyltriethoxysilane (FAS-17) was selected to modify SiO_2. FAS-17 has a long carbon chain and 17 fluorine atoms in its molecule. It can react with SiO_2 to form Si-O-Si bonds under alkaline conditions [37]. The agglomeration of NPs is alleviated from two points. The long carbon chain increases the steric hindrance [41]. Seventeen fluorine atoms greatly reduce the surface energy [27].

In this article, first, FAS-17-modified nano-SiO_2 was prepared. Then, PDMS was used as the low-surface-energy substrate, and FAS-17 was used to fabricate the FAS-17-modified SiO_2/PDMS super-hydrophobic interface. Meanwhile, the agglomeration mechanism of nano-SiO_2 and the super-hydrophobic mechanism of FAS-17-modified SiO_2/PDMS coatings were analyzed. In order to evaluate the insulating properties, the breakdown voltage of the super-hydrophobic coatings was tested.

2. Experiment

2.1. Materials

TetraEthyl Orthosilicate (TEOS, analytically pure) and Dibutyltin Dilaurate (analytically pure) were both obtained from Shanghai Macklin Biochemical Co., Ltd. (Shanghai, China).

The 107 RTV-silicone rubber (PDMS, analytically pure) was purchased from Shanghai Aladdin Biochemical Technology Co., Ltd. (Shanghai, China).

1H, 1H, 2H, 2H-perfluorodecyltriethoxysilane (FAS-17, analytically pure) was purchased from Shanghai Bide Medical Technology Co., LTD. (Shanghai, China).

Anhydrous ethanol (analytically pure) and ammonia solution (analytically pure, 26 wt %) were purchased from Shanghai Aladdin Biochemical Technology Co., Ltd. (Shanghai, China)

All chemicals were used as received without any further purification.

2.2. Instrument and Apparatus

Vacuum drying oven and air pump (Shanghai Jing Hong Experimental Equipment Co., LTD., Shanghai, China); spray pen (Taiwan U-Star spraying tools Co., Ltd., Taiwan, China); OCA20 contact angle tester (DataPhysics Instruments GmbH, Filderstadt, Germany); Nicolet 5700 FT-IR (Thermo Fisher Scientific Inc., Waltham, MA, USA); Nova Nano SEM450 (Thermo Fisher Scientific Inc., Waltham, MA, USA); Ultim Extreme EDS (Oxford Instrument, London, UK); BTS-75 breakdown voltage tester (Beijing Xing Di Instrument Co., LTD., Beijing, China).

2.3. Method

2.3.1. The Preparation of Nano-SiO_2

Nano-SiO_2 was prepared using the Stöber method [42].

In detail, first, 2.0 g of TEOS, 40.0 g of CH_3CH_2OH, 4.0 g of H_2O, and 0.30 g of $NH_3 \cdot H_2O$ (the catalyst) were added into a three-hole flask and heated at 45 °C with magnetic stirring at 1000 rpm or 4.5 h. Thus, the nano-SiO_2 was obtained.

2.3.2. The Preparation of FAS-17-Modified Nano-SiO_2

A total of 5 g of nano-SiO_2 was dissolved in 100 mL of a 95% ethanol–water solution in a beaker. Then, the beaker was placed in an ultra-sonic atmosphere to obtain a transparent white emulsion. After 20 min, the mixture was transferred into a 250 mL three-hole flask. Then, 0.25 g of FAS-17 and 0.1 g of $NH_3 \cdot H_2O$ were added into the flask. Then, the dispersion was heated at 70 °C under magnetic stirring for 5 h. Then, the mixture was heated in a vacuum oven for 6 h. Finally, the mixture was ground into a white powder.

Figure 1 briefly shows the principle of synthesizing FAS-17-modified nano-SiO_2.

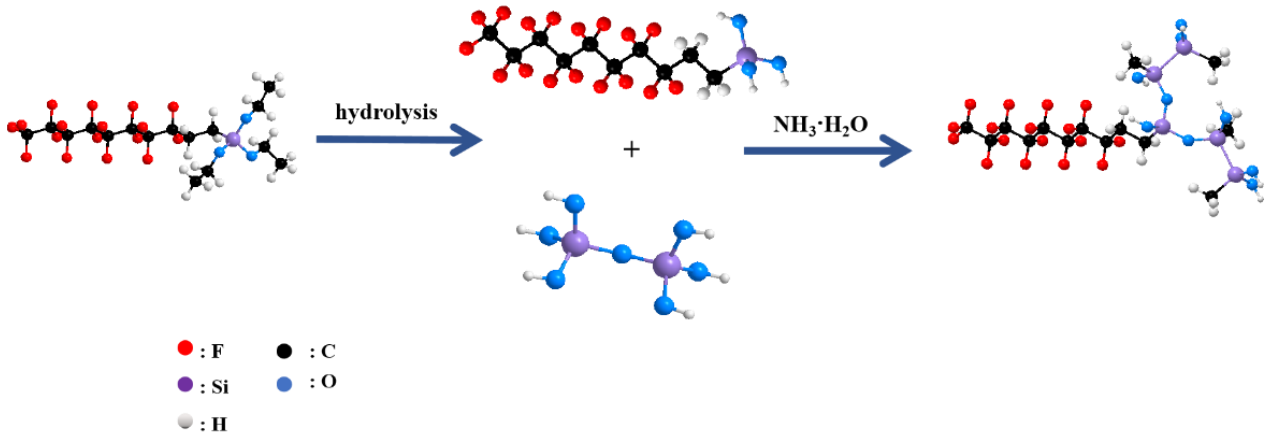


Figure 1. Schematic diagram of the construction of a porous FAS-17-modified SiO_2.

2.3.3. The Preparation of Super-Hydrophobic Coating

A total of 10 g of PDMS was added into the beaker and dissolved in n-hexane. After magnetic stirring for 15 min, 1 g of dibutyltin dilaurate was added to the solution. A pre-cleaned insulator silicone rubber was laid flat on a glass plate. Then, the solution was poured onto the silicone and heated in the vacuum oven for 0.5 h at 80 °C to let it half dry. FAS-17-modified nano-SiO_2 was dissolved in ethyl alcohol. Then, the solution was sprayed onto the surface of PDMS with a spray pen. Finally, the silicone rubber was heated in the vacuum oven at 100 °C for 2 h, and the super-hydrophobic RTV-silicone rubber was obtained.

Figure 2 briefly shows the construction process of FAS-17-modified nano-SiO_2/PDMS coatings.

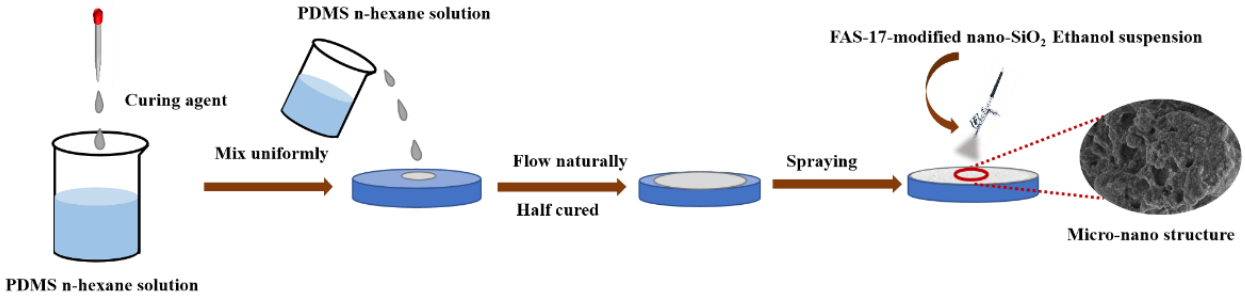


Figure 2. Schematic diagram of the fabrication of FAS-17-modified nano-SiO_2/PDMS protective coatings on composite insulators.

2.3.4. The Preparation to Calculate the Binding Energy

Binding energy (BE) is the energy released when several particles combine from a free state into a composite particle that can be used to evaluate the firm degree of molecular binding.

In quantum chemistry, it can be calculated by substituting the equation $E_{BE} = E_{comp} - \sum E_{mon}$ into the binding energies of the compound (comp) and monomer (mono), where E_{BE} is the binding energy of two molecules, E_{comp} is the adsorption energy of the compound, and E_{mono} is the adsorption energy of the monomer that builds the compound.

The binding energy between two molecules and the energy of the monomer were calculated through the Gaussian16 software package using the density functional theory (DFT). The M06-2X density function and the def2-TZVP basis set were used to optimize the structure and calculate the energy.

2.4. Characterization

A contact angle–measuring instrument equipped with a tilting table was used to measure the contact angle and sliding angle. Three random parts on the surface of the sample were used for testing. The volume of the droplets to test the contact angle was 2 μL. The volume of the droplets to test the sliding angle was 10 μL.

Nova Nano SEM450 SEM (Thermo Fisher Scientific Inc., Tokyo, Japan) was used to investigate the morphology of the samples. The extraction voltage was 5.00 KV. All the samples were previously metalized for 2 min using a high-resolution sputtering coating instrument Q150T S (Quorum Technologies, Chico, CA, USA).

Ultim Extreme EDS (Oxford Instrument, London, UK) was used to characterize the elemental composition and content of the samples.

Nicolet 5700 FT-IR (Thermo Fisher Scientific Inc., Waltham, MA, USA) was used to illustrate the successful introduction of fluorine on SiO_2.

2.5. Performance Testing

Power Grid Security Test

In order to evaluate the anti-pollution flashover performance, the breakdown voltage of the FAS-17-modified nano-SiO_2–coated silicone rubber composite insulator was tested using a BTS-75 breakdown voltage tester (Beijing Xing Di Instrument Co., Ltd., Beijing, China). The rapid uniform voltage boost method was used to raise the voltage, and the voltage boost speed was 1 kV/s.

3. Results and Discussion

3.1. Analysis of Surface Morphology and Elemental Distribution

By observing Figure 3a,b, the surface of the composite insulator has many cracks and is relatively smooth without a rough transparent structure. Figure 3c–f are the SEM images of the PDMS surface. There are fewer cracks in the PDMS surface. It can be seen from the SEM image that the micro-nanoscale, mastoid-like structure on the primer substrate was formed by the atomization effect in the spraying process, in which the

introduction of FAS-17-modified nano-SiO_2 played a critical role. Many holes were found in the micro-nanostructure. The scale of the holes is around 20–60 nm. The primer PDMS substrate obtained in the absence of FAS-17-modified nano-SiO_2 is relatively flat without any mastoid-like structure.

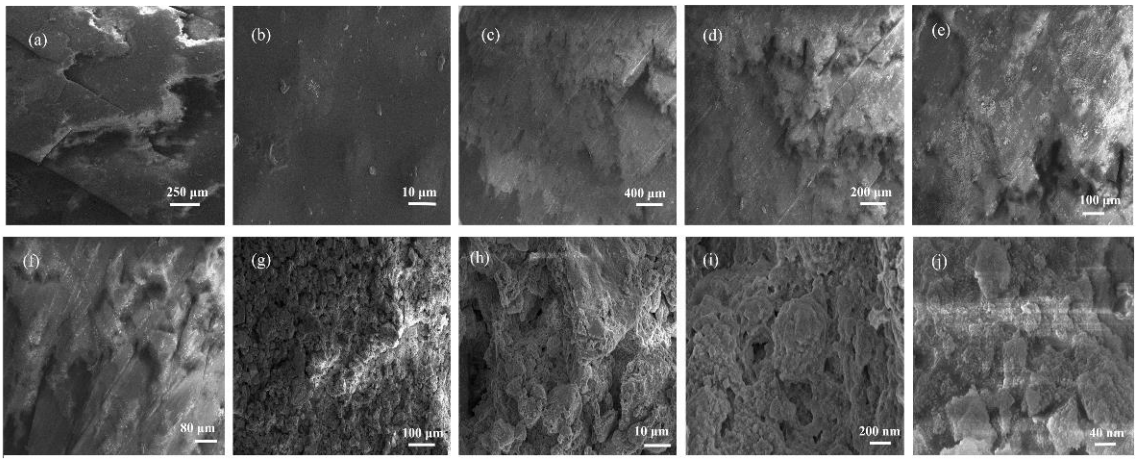


Figure 3. (**a**) SEM images of the surface of composite insulator. (**b**) Magnified SEM images of the surface of composite insulator. (**c**) SEM images of PDMS surface. (**d**–**f**) Magnified SEM images of PDMS surface. (**g**) SEM images of FAS-17-modified nano-SiO_2/PDMS surface. (**h**–**j**) Magnified SEM images of FAS-17-modified nano-SiO_2 /PDMS surface.

Figure 4a shows the EDS diagram and elemental distribution of the composite insulator. It can be seen that the main element on the surface are C, O, Ca, and Fe. The elements Na, F, Cl, and Al are the minorities.

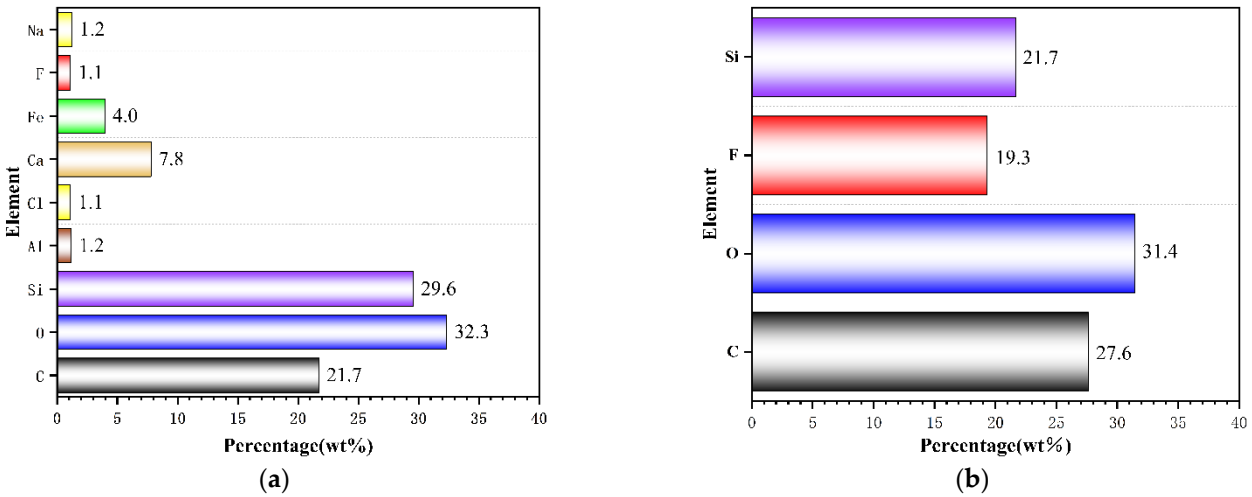


Figure 4. (**a**) Elemental distribution of composite insulator. (**b**) Elemental distribution of FAS-17-modified nano-SiO_2/PDMS surface.

3.2. Analysis of Super-Hydrophobic Coating

The super-hydrophobic coatings constructed on the surface of the composite insulator were achieved by sequentially naturally flowing flat PDMS (used as a low-surface-energy material) and spray-depositing FAS-17-modified nano-SiO_2 (used to increase surface roughness) on it. The successful introduction of fluorocarbon groups can be confirmed by the FT-IR spectra. Compared with the FT-IR spectra of SiO_2, FAS-17-modified SiO_2 shows adsorption bands at 1238, 1210, and 1145 cm^{-1}, which are attributed to the C-F stretching vibration of the -CF_3 and -CF_2- groups in the fluorinated alkyl chains (Figure 5). By compar-

ing Figure 4b with Figure 4a, it can be found that the rate of the F element increased sharply, which indicates that the FAS-17-modified nano-SiO_2/PDMS were successfully constructed.

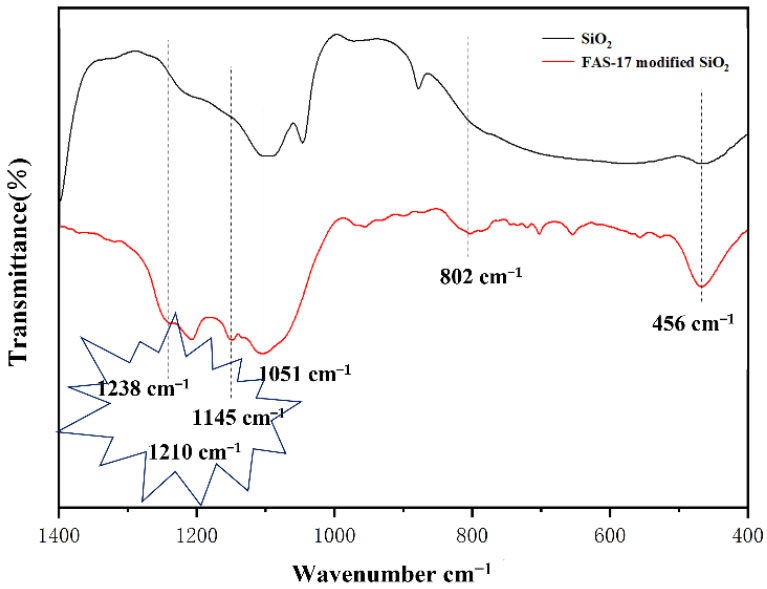


Figure 5. FT-IR spectra of SiO_2 and FAS-17-modified SiO_2.

3.3. SiO_2 Agglomeration Mechanism and FAS-17-Modified Nano-SiO_2 De-Agglomeration Mechanism

The agglomeration of NPs can be divided into two states: hard aggregate and soft aggregate. The formation of hard agglomerations is mainly influenced by electrostatic forces, van der Waals forces, and chemical bonds. Soft agglomerations are mainly caused by electrostatic forces and van der Waals forces between particles or capillary forces due to the presence of liquid in the agglomerations.

Theoretically, the whole motion process of NPs agglomeration can be divided into three stages:

(a) Particles approach the phase of motion;
(b) Contact phase;
(c) Agglomerative growth stage.

The classic DLVO theory describes the change in the total interaction energy experienced by one nanoparticle as it approaches another. The theory is shown as the following formula (V_A is a short-range attractive van der Waals potential, and V_R is a long-range repulsive electrostatic potential) [43–45], Table 1 shows the meaning of the symbols of the DLVO theory.

$$V_{total} = V_A + V_R \quad (1)$$

where

$$V_R = -\frac{AR}{12D} + 2\pi\varepsilon\varepsilon_0\Psi^2 e^{-kD} \quad (2)$$

where

$$\kappa K = \left[\sum_i \frac{z_i^2 q_i^2 c_i^2}{k_B T}\right]^2 \quad (3)$$

From the above formula, we can see that the calculation process of the DLVO theory is extremely complex and not intuitive.

Therefore, to directly and quantitatively express the reason why the modified molecules are not easy to agglomerate, the binding energy of SiO_2, two SiO_2 molecules, and two FAS-17-modified SiO_2 molecules were calculated.

Table 1. Symbols of the DLVO theory.

Symbol	Meaning of the Symbols
A	Hamaker constant
R	Radius of the particles
ε_o	Permittivity of vacuum
ε	Dielectric constant of the solvent
ψ	Stern potential
k	Debye constant
z_i	Charge number of the ionic species
i	Elementary charge
c_i	Concentration of ion i (co- or counter-ions) at x = ∞ (in the bulk solution)
k_B	Boltzmann constant
T	Temperature of the system

As shown in Figure 6, the binding energy of two SiO_2 molecules was −2219.10 kcal·mol^{-1}, and the binding energy of two FAS-17-modified SiO_2 molecules was −9040.26 kcal·mol^{-1}. After modification, the binding energy of the molecules decreased sharply, which indicates that the two FAS-17-modified SiO_2 molecules were not attracted to each other. This is because FAS-17 has a unique molecular structure. As a molecule rich in fluorine, it has a rather low surface energy. The long fluorine–carbon chain in the molecule acts as a barrier, which greatly increases the steric hindrance. The large steric hindrance prevents the agglomeration of modified molecules.

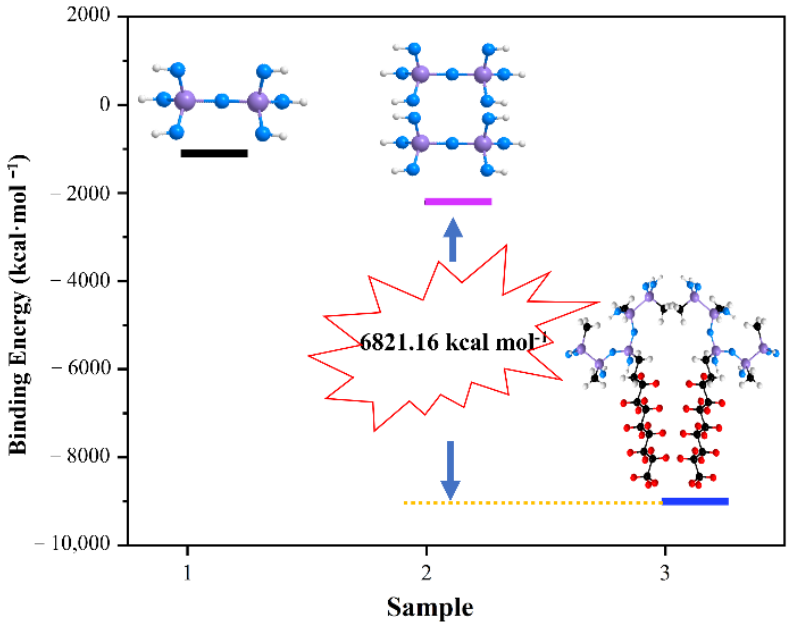


Figure 6. Diagram of binding energy (1-SiO_2, 2-two SiO_2 molecules, 3-two FAS-17-modified SiO_2 molecules).

3.4. Super-Hydrophobic Mechanism

As for the super-hydrophobic mechanism of the super-hydrophobic coating, previous reports were mostly interpreted from the low-surface-energy substrate of the coating and the introduction of nanoparticles to increase the roughness.

In our work, PDMS was the low-surface-energy substrate. After merely introducing it on the composite insulator surface, the hydrophobicity of the composite insulator was improved to a certain extent. As shown in Figure 7a,b, the shape of the water droplet on the surface changed from a hemisphere to three-quarters of a sphere, which means that the droplet's ability to roll on the surface was further improved. Further contact angle and rolling angle tests showed that (see Figure 8), after modification, the angle of droplet rolling

was greatly reduced (see Figure 9), the contact angle increased from 104.1° to 115.9°, and the sliding angle decreased from 151.6° to 19.2°.

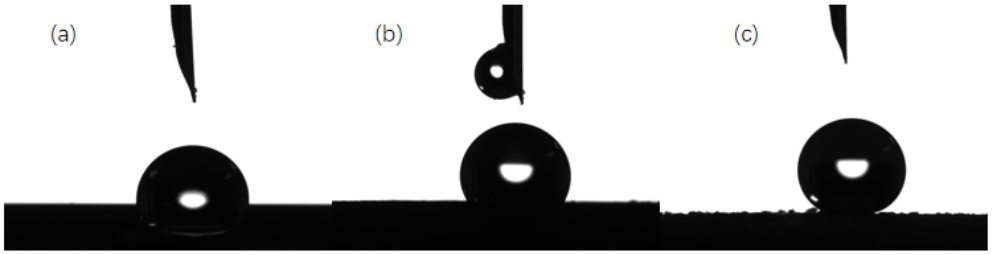


Figure 7. Water droplet shape on (**a**) insulator surface, (**b**) PDMS surface, and (**c**) FAS-17-modified nano-SiO_2/PDMS surface.

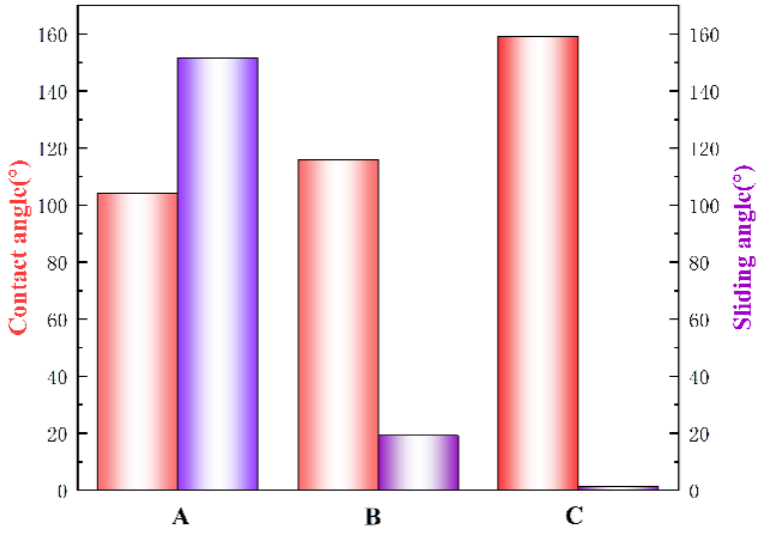


Figure 8. Contact angle and sliding angles of samples **A**, **B,** and **C** (**A**—insulator; **B**—PDMS; **C**—FAS-17-modified nano-SiO_2/PDMS).

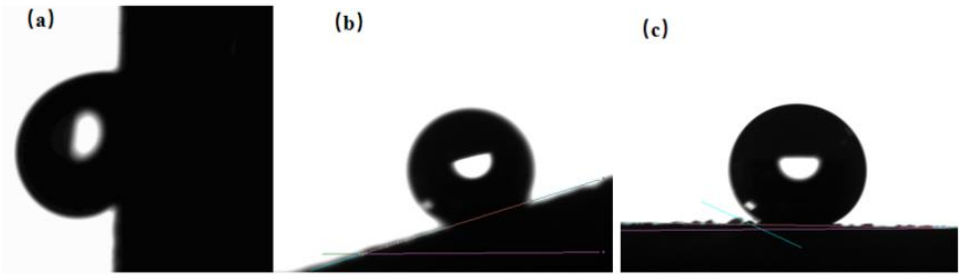


Figure 9. Water droplet shape showing roll angles on (**a**) insulator surface, (**b**) PDMS surface, and (**c**) FAS-17-modified nano-SiO_2/PDMS surface.

After spraying FAS-17-modified nano-SiO_2 particles on the surface of PDMS, water droplets gained greater possibilities for movement. The shape of the water droplet on the FAS-17-modified nano-SiO_2/PDMS surface was very nearly spherical (see Figure 7c). The contact angle increased from 115.9° to 159.2°, and the sliding angle decreased from 19.2° to 1.3°, which indicates that the coatings gained super-hydrophobic properties and a slight disturbance to the surface of the coating could cause the water droplets to move. It can be seen from Table 2 that the contact angle of the prepared FAS-17-modified SiO_2/PDMS coatings is in the middle of those of other standard hydrophobic surfaces from the literature.

Table 2. Standard hydrophobic surfaces from literature.

Materials	Method	Contact Angle	Reference
Porous SiO_2@PDMS layer; FAS-modified ceramic membranes	Spraying	155.8°	[39]
SiO_2 nanoparticle	Spraying	151.5°	[40]
Nanosized silica hollow spheres; PDMS	Template method	160°	[46]
PDMS@304SS mesh	Chemical etching	159°	[47]

In order to further explain the variation of hydrophobicity of the coating surface, the binding energy of the coating with water, before and after modification, was calculated. (Figure 10). It is obvious that, after modification, the binding energy decreased sharply from −1185.92 kcal·mol^{-1} to −4596.55 kcal·mol^{-1}. The low surface binding energy made the adsorption capacity of the modified coating for water very weak, which allowed the water droplet to move freely.

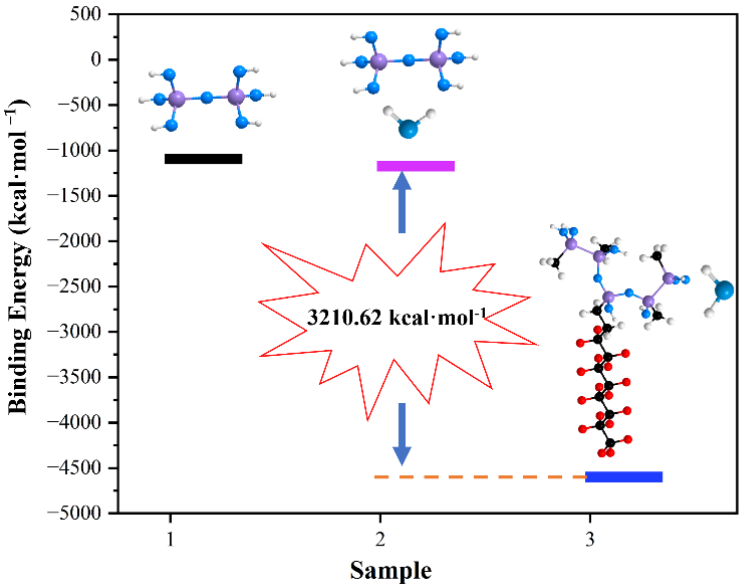


Figure 10. Diagram of adsorption energy (1—SiO_2; 2—SiO_2 molecular and H_2O; 3—FAS-17-modified SiO_2 molecular and H_2O).

3.5. High-Voltage Safety Evaluation

In order to evaluate the electrical insulation performance of FAS-17-modified SiO_2/PDMS samples, the breakdown voltage (the voltage at which the sample breaks down in a continuous boost test) of the samples was tested.

After the breakdown, the current in the loop increases, and the voltage at both ends of the sample drops. The transformer console jumps because of the circuit breaker action and records the maximum test voltage displayed by the capacitor voltage divider. Two kinds of different silicone rubber samples were tested successively, and there were three samples for each. The average value of the three test results was taken to obtain the breakdown voltage of the silicone rubber sample at a room temperature of 20 °C.

It can be seen from Figure 11 that the breakdown voltage of the two types of silicone rubber insulators that the breakdown voltage of the insulator after super-hydrophobic modification was slightly increased from 6.1 kV to 6.8 kV, and the modification was conducive to improving the insulation performance of the insulator.

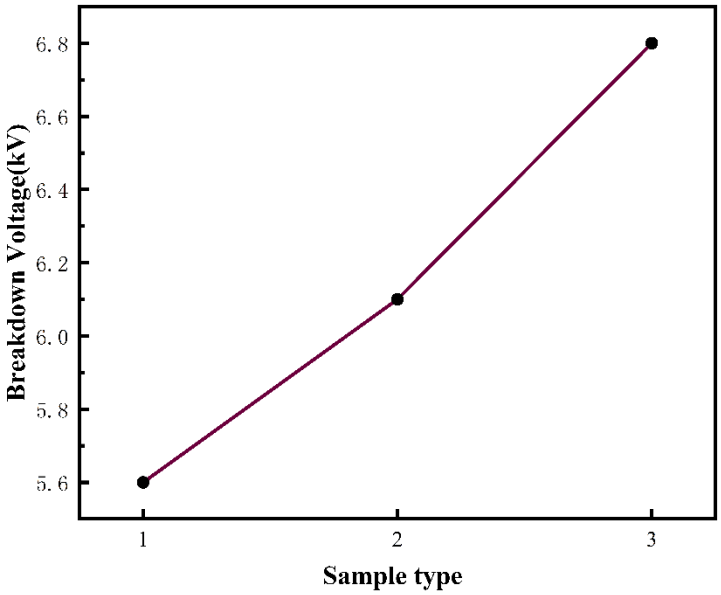


Figure 11. Breakdown voltage of different samples (1—insulator; 2—PDMS/insulator; 3—FAS-17-modified nano-SiO_2 PDMS/insulator).

4. Conclusions

In this study, using the physical deposition method, the synthesis of FAS-17-modified nano-SiO_2/PDMS super-hydrophobic coatings was achieved. The contact angle and sliding angle of the super-hydrophobic coating were optimized to 159.2°and 1.3°, respectively. The mechanism of the easy agglomeration of NPs before modification and the difficult agglomeration of NPs after modification was investigated. The hydrophobic mechanism of the super-hydrophobic coating was explained using a computer simulation. The super-hydrophobic coating has superior self-cleaning properties and outstanding electrical insulation properties that can meet the need for high-voltage insulators. Meanwhile, the process of constructing the coating is rather simple, making it more feasible for application in industry.

Above all, the coatings have great prospects for preventing insulator flashover and decreasing the washing frequency for high-grid power line insulators.

Author Contributions: Methodology, C.L., P.D., and B.S.; Software, C.L. and R.Z.; Validation, C.L., Y.S. and G.F.; Formal analysis, R.Z. and B.S.; Investigation, C.L.; Data curation, C.L. and R.Z.; Writing—original draft, C.L.; Writing—review & editing, B.S.; Supervision, B.S.; Project administration, P.D. All authors have read and agreed to the published version of the manuscript.

Funding: The work was supported by funds from the Jiangsu Frontier Electric Power Enterprise Fund project CX202115.

Institutional Review Board Statement: Not applicable.

Informed Consent Statement: Not applicable.

Data Availability Statement: Data is contained within the article.

Conflicts of Interest: The authors declare no conflict of interest.

References

1. Sun, J.; Hu, Y.; Jiang, X.; Wu, Y.; Li, T.; Zhao, Y.; Rong, Y. Discharge development process and flashover performance of snow-accreted insulators under natural environment. *Int. J. Electr. Power Energy Syst.* **2023**, *146*, 108678. [CrossRef]
2. Bahrami, A.; Yan, M.; Shahidehpour, M.; Pandey, S.; Vukojevic, A.; Paaso, E.A. Mobile and Portable De-Icing Devices for Enhancing the Distribution System Resilience Against Ice Storms: Preventive strategies for damage control. *IEEE Electrif. Mag.* **2021**, *9*, 120–129. [CrossRef]

3. Gomila, D.; Carreras, B.A.; Reynolds-Barredo, J.M.; Colet, P.; Gomis-Bellmunt, O. Analysis of the blackout risk reduction when segmenting large power systems using lines with controllable power flow. *Int. J. Electr. Power Energy Syst.* **2023**, *148*, 108947. [CrossRef]
4. Salem, A.A.; Lau, K.Y.; Abdul-Malek, Z.; Al-Gailani, S.A.; Tan, C.W. Flashover voltage of porcelain insulator under various pollution distributions: Experiment and modeling. *Electr. Power Syst. Res.* **2022**, *208*, 107867. [CrossRef]
5. Wang, W.; Lu, H.; Li, C.; Deng, Y.; Lan, L.; Wen, X.; Luo, B.; Xiao, W. Study on the relationship between the characteristics of water droplets on the shed of composite insulators and the pollution flashover voltage. *Energy Rep.* **2022**, *8*, 1071–1077. [CrossRef]
6. Li, Z.; Yin, F.; Cao, B.; Wang, L.; Shao, S.; Farzaneh, M. Pollution flashover performance of RTV coatings with partial damage. *Int. J. Electr. Power Energy Syst.* **2020**, *121*, 106102. [CrossRef]
7. Mohammadnabi, S.; Rahmani, K. Influence of humidity and contamination on the leakage current of 230-kV composite insulator. *Electr. Power Syst. Res.* **2021**, *194*, 107083. [CrossRef]
8. Liu, Y.; Zong, H.; Gao, S.; Du, B.X. Contamination deposition and discharge characteristics of outdoor insulators in fog-haze conditions. *Int. J. Electr. Power Energy Syst.* **2020**, *121*, 106176. [CrossRef]
9. Mohammadi Savadkoohi, E.; Mirzaie, M.; Seyyedbarzegar, S.; Mohammadi, M.; Khodsuz, M.; Ghorbani Pashakolae, M.; Biazar Ghadikolaei, M. Experimental investigation on composite insulators AC flashover performance with fan-shaped non-uniform pollution under electro-thermal stress. *Int. J. Electr. Power Energy Syst.* **2020**, *121*, 106142. [CrossRef]
10. Subba Reddy, B.; Ramamurthy, P.C. Analysis of in-service composite insulators used in overhead railway traction. *Eng. Fail. Anal.* **2020**, *108*, 104227. [CrossRef]
11. Qiao, X.; Zhang, Z.; Jiang, X.; Sundararajan, R.; You, J. DC pollution flashover performance of HVDC composite insulator under different non-uniform pollution conditions. *Electr. Power Syst. Res.* **2020**, *185*, 106351. [CrossRef]
12. Li, X.; Tian, J.; Ma, Z.; Zhou, W.; Qin, Y. Numerical Analysis and Experimental Study of the Laser Cleaning of Ceramic Insulator Contamination. *IEEE Access* **2022**, *10*, 49285–49296. [CrossRef]
13. Máša, V.; Horňák, D.; Petrilák, D. Industrial use of dry ice blasting in surface cleaning. *J. Clean. Prod.* **2021**, *329*, 129630. [CrossRef]
14. Baghshahi, S.; Mohammadi, M.; Payrazm, S.; Aliabadizadeh, A. Hydrophobic nanocrystalline glazes based on cassiterite for self-cleaning outdoor power grid insulators. *J. Eur. Ceram. Soc.* **2021**, *41*, 5750–5754. [CrossRef]
15. Plieva, M.; Gurieva, E.; Lysokon, E. Analysis of Different Modes of Cleaning Insulators of Air Transmission Lines in Mountain Conditions. In Proceedings of the 2020 International Ural Conference on Electrical Power Engineering (UralCon), Chelyabinsk, Russia, 22–24 September 2020.
16. Mittal, T. Self-cleaning smart photocatalytic coatings for water treatment. *Mater. Today Proc.* **2022**, *in press*. [CrossRef]
17. Wang, X.; Ding, H.; Lv, G.; Zhou, R.; Ma, R.; Hou, X.; Zhang, J.; Li, W. Fabrication of superhydrophilic self-cleaning SiO_2–TiO_2 coating and its photocatalytic performance. *Ceram. Int.* **2022**, *48*, 20033–20040. [CrossRef]
18. Wang, K.; Yu, S.; Li, W.; Song, Y.; Gong, P.; Zhang, M.; Li, H.; Sun, D.; Yang, X.; Wang, X. Superhydrophobic and photocatalytic synergistic Self-Cleaning ZnS coating. *Appl. Surf. Sci.* **2022**, *595*, 153565. [CrossRef]
19. Wang, S.; Li, L.; Zou, Q.; Chen, J.; Zhao, X.; Xie, Y.; Hu, Y.; Yang, K. Abrasion mechanisms of superhydrophobic coating surfaces wetted in Wenzel state. *Colloids Surf. A Physicochem. Eng. Asp.* **2023**, *657*, 130585. [CrossRef]
20. Chen, X.; Hu, L.; Du, Y. Anti-icing and anti-frost properties of structured superhydrophobic coatings based on aluminum honeycombs. *Mater. Chem. Phys.* **2022**, *291*, 126683. [CrossRef]
21. Aparna, A.; Sethulekshmi, A.S.; Saritha, A.; Joseph, K. Recent advances in superhydrophobic epoxy based nanocomposite coatings and their applications. *Prog. Org. Coat.* **2022**, *166*, 106819. [CrossRef]
22. Selim, M.S.; El-Safty, S.A.; Shenashen, M.A. Chapter 8-Superhydrophobic foul resistant and self-cleaning polymer coating. In *Superhydrophobic Polymer Coatings*; Samal, S.K., Mohanty, S., Nayak, S.K., Eds.; Elsevier: Amsterdam, The Netherlands, 2019; pp. 181–203.
23. He, G.; Wan, M.; Wang, Z.; Zhao, Y.; Sun, L. Fabrication of firm, superhydrophobic and antimicrobial PVDF@ZnO@TA@DT electrospun nanofibrous membranes for emulsion separation. *Colloids Surf. A Physicochem. Eng. Asp.* **2023**, *662*, 130962. [CrossRef]
24. Wang, X.; Wang, B.-B.; Yang, W.; Zhao, Q.; Xu, Z.-M.; Yan, W.-M. Fabrication of stable and versatile superhydrophobic PTFE coating by simple electrodeposition on metal surface. *Prog. Org. Coat.* **2022**, *172*, 107090. [CrossRef]
25. Cui, Y.; Liu, H.; Wei, B.; Deng, C.; Bai, Y. Fabrication of UV-curable Anti-fouling coating based on fluorinated polyoxetane and long Side-Chain Polysilcone. *Eur. Polym. J.* **2022**, *172*, 111227. [CrossRef]
26. Gupta, R.; Verma, R.; Kango, S.; Constantin, A.; Kharia, P.; Saini, R.; Kudapa, V.K.; Mittal, A.; Prakash, J.; Chamoli, P. A critical review on recent progress, open challenges, and applications of corrosion-resistant superhydrophobic coating. *Mater. Today Commun.* **2023**, *34*, 105201. [CrossRef]
27. Singh, A.K. Surface engineering using PDMS and functionalized nanoparticles for superhydrophobic coatings: Selective liquid repellence and tackling COVID-19. *Prog. Org. Coat.* **2022**, *171*, 107061. [CrossRef]
28. Liu, Y.; Guo, R.; Liu, J.; Zhang, Q. Robust PFMA/CNTs composite PDMS superhydrophobic film via SI-CuCRP method for efficient anti-icing. *Colloids Surf. A Physicochem. Eng. Asp.* **2023**, *660*, 130913. [CrossRef]
29. Wang, Q.; Sun, G.; Tong, Q.; Yang, W.; Hao, W. Fluorine-free superhydrophobic coatings from polydimethylsiloxane for sustainable chemical engineering: Preparation methods and applications. *Chem. Eng. J.* **2021**, *426*, 130829. [CrossRef]
30. Armugam, A.; Teong, S.P.; Lim, D.S.W.; Chan, S.P.; Yi, G.; Yew, D.S.; Beh, C.W.; Zhang, Y. Broad spectrum antimicrobial PDMS-based biomaterial for catheter fabrication. *Biomater. Res.* **2021**, *25*, 33. [CrossRef] [PubMed]

31. Liu, J.; Yao, Y.; Li, X.; Zhang, Z. Fabrication of advanced polydimethylsiloxane-based functional materials: Bulk modifications and surface functionalizations. *Chem. Eng. J.* **2021**, *408*, 127262. [CrossRef]
32. Zhang, W.; Gao, N.; Li, J.; Wu, H.; Izuchukwu, N.K.; Ahmed, S.; Han, E.-H.; Liu, F. Enhanced anti-icing and anticorrosion properties of nano-SiO_2 composite superhydrophobic coating constructed by a large-scale micropillar array approach. *Prog. Org. Coat.* **2023**, *175*, 107324. [CrossRef]
33. Liang, T.; Guo, X.; Yuan, B.; Kong, S.; Huang, H.; Fu, D.; Zhang, F.; Xu, J.; Li, X. Design of functionalized α-Fe_2O_3 (III) films with long-term anti-wetting properties. *Ceram. Int.* **2020**, *46*, 6129–6135. [CrossRef]
34. Xu, Z.; Xu, L.; Wang, Y.; Li, Q.; Cui, S.; Nie, Z.; Wei, Q. Growing nearly vertically aligned ZnO nanorod arrays on porous α-Al_2O_3 membranes to enhance the separation of MTBE from aqueous solution. *Sep. Purif. Technol.* **2023**, *311*, 123239. [CrossRef]
35. Khaled, U.; Beroual, A. Lightning impulse breakdown voltage of synthetic and natural ester liquids-based Fe_3O_4, Al_2O_3 and SiO_2 nanofluids. *Alex. Eng. J.* **2020**, *59*, 3709–3713. [CrossRef]
36. Guo, G.; Zhang, J.; Chen, X.; Zhao, X.; Deng, J.; Zhang, G. Molecular-dynamics study on the thermodynamic properties of nano-SiO_2 particle-doped silicone rubber composites. *Comput. Mater. Sci.* **2022**, *212*, 111571. [CrossRef]
37. Liu, M.; Tan, X.; Li, X.; Geng, J.; Han, M.; Wei, K.; Chen, X. Transparent superhydrophobic EVA/SiO_2/PTFE/KH-570 coating with good mechanical robustness, chemical stability, self-cleaning effect and anti-icing property fabricated by facile dipping method. *Colloids Surf. A Physicochem. Eng. Asp.* **2023**, *658*, 130624. [CrossRef]
38. Du, J.; Yuan, H.; Xia, H.; Kou, H.; Zhang, Y.; Xing, W.; Zhang, C. Improvement of superhydrophobicity and durability of EP+PDMS/SiO_2 composite coatings by adjusting laser curing powers. *Mater. Chem. Phys.* **2022**, *289*, 126428. [CrossRef]
39. Dai, X.; Wei, Q.; Wang, Y.; Li, Q.; Cui, S.; Nie, Z. A novel strategy to enhance the desalination stability of FAS (fluoroalkylsilane)-modified ceramic membranes via constructing a porous SiO_2@PDMS (polydimethylsiloxane) protective layer on their top. *Chem. Eng. J.* **2022**, *435*, 134757. [CrossRef]
40. Rius-Ayra, O.; Biserova-Tahchieva, A.; Sansa-López, V.; Llorca-Isern, N. Superhydrophobic PDMS coated 304 stainless-steel mesh for the removal of HDPE microplastics. *Prog. Org. Coat.* **2022**, *170*, 107009. [CrossRef]
41. Yang, Y.; Shan, L.; Shen, H.; Qiu, J. Manufacturing of robust superhydrophobic Wood surfaces based on PEG–Functionalized SiO_2/PVA/PAA/Fluoropolymer hybrid transparent coating. *Prog. Org. Coat.* **2021**, *154*, 106186. [CrossRef]
42. Sivolapov, P.; Myronyuk, O.; Baklan, D. Synthesis of Stober silica nanoparticles in solvent environments with different Hansen solubility parameters. *Inorg. Chem. Commun.* **2022**, *143*, 109769. [CrossRef]
43. Kolb, C.G.; Lehmann, M.; Kulmer, D.; Zaeh, M.F. Modeling of the stability of water-based graphite dispersions using polyvinylpyrrolidone on the basis of the DLVO theory. *Heliyon* **2022**, *8*, e11988. [CrossRef] [PubMed]
44. Shi, Z.; Ran, B.; Liu, L. Determining the interaction energy of a quartz–kaolinite system at different pH levels by atomic force microscopy and extended DLVO theory. *Powder Technol.* **2022**, *409*, 117842. [CrossRef]
45. de Lima, S.L.S.; Miguel, V.M.; Rosado, T.F.; Petri, M.V.; Gardener, J.; Avillez, R.; Rodrigues, T.S.; de Torresi, S.I.C.; Solorzano, G.; da Silva, A.G.M. Sized-controlled Pd nanoflowers by a non-classical growth mechanism combining the LaMer and DLVO theories and their catalytic activities. *Mater. Today Commun.* **2022**, *33*, 104397. [CrossRef]
46. Yu, X.; Liu, X.; Shi, X.; Zhang, Z.; Wang, H.; Feng, L. SiO_2 nanoparticle-based superhydrophobic spray and multi-functional surfaces by a facile and scalable method. *Ceram. Int.* **2019**, *45*, 15741–15744. [CrossRef]
47. Sun, Y.; Zhao, H.; Mao, H.; Duan, M.; Wang, K.; Bao, N.; Zhao, Z.-P.; Li, H. Silica hollow spheres-based superhydrophobic PDMS composite membrane for enhanced acetone permselective pervaporation. *Sep. Purif. Technol.* **2023**, *304*, 122041. [CrossRef]

Disclaimer/Publisher's Note: The statements, opinions and data contained in all publications are solely those of the individual author(s) and contributor(s) and not of MDPI and/or the editor(s). MDPI and/or the editor(s) disclaim responsibility for any injury to people or property resulting from any ideas, methods, instructions or products referred to in the content.